

Electronic Supplemental Information for

**Pyridine-functionalized Fullerene Additive Enabling Coordination
Interactions with CH₃NH₃PbI₃ Perovskite towards Highly Efficient
Bulk Heterojunction Solar Cells**

Jieming Zhen^{#a}, Weiran Zhou^{#a}, Muqing Chen^{*#a}, Bairu Li^a, Lingbo Jia^a, Mingtai Wang^b, and Shangfeng Yang^{*a}

^aHefei National Laboratory for Physical Sciences at Microscale, CAS Key Laboratory of Materials for Energy Conversion, Department of Materials Science and Engineering, Synergetic Innovation Center of Quantum Information & Quantum Physics, University of Science and Technology of China, Hefei 230026, China.

E-mail: mqchen@ustc.edu.cn (M. C.); sfyang@ustc.edu.cn (S.Y.)

^bInstitute of Applied Technology, Hefei Institutes of Physical Science, Chinese Academy of Sciences, Hefei 230088, China

[#] These authors contributed equally to this work.

Contents

- S1. ^1H NMR and ^{13}C NMR spectrum of $\text{C}_{60}\text{-PyP}$.**
- S2. Mass spectrum of $\text{C}_{60}\text{-PyP}$.**
- S3. Estimation of the energy levels of $\text{C}_{60}\text{-PyP}$.**
- S4. TGA analysis of $\text{C}_{60}\text{-PyP}$.**
- S5. UV-vis spectra of the MAPbI_3 perovskite with varying $\text{C}_{60}\text{-PyP}$ concentration.**
- S6. PCE histograms of the control and 0.13 wt% devices.**
- S7. Photovoltaic parameters box plots of devices with varying $\text{C}_{60}\text{-PyP}$ concentration.**
- S8. Hysteresis characterization of devices with and without 0.13 wt% $\text{C}_{60}\text{-PyP}$.**
- S9. Histograms of grain size distributions of the MAPbI_3 perovskite film with varying $\text{C}_{60}\text{-PyP}$ concentration.**
- S10. XPS profile of I 3d of the $\text{CH}_3\text{NH}_3\text{PbI}_3$ perovskite films without and with 1.0 wt% $\text{C}_{60}\text{-PyP}$ doping**
- S11. Analysis of time-resolved photoluminescence (TRPL) spectra of the perovskite films with or without $\text{C}_{60}\text{-PyP}$.**
- S12. Fitted EIS data for Control and 0.13 wt% devices.**
- S13. J-V curves and the stabilized photocurrent densities and power outputs measured at the maximum power.**
- S14. Ambient stabilities of the control and $\text{C}_{60}\text{-PyP}$ doped perovskite films.**

S1. ^1H NMR and ^{13}C NMR spectrum of C_{60} -PyP.

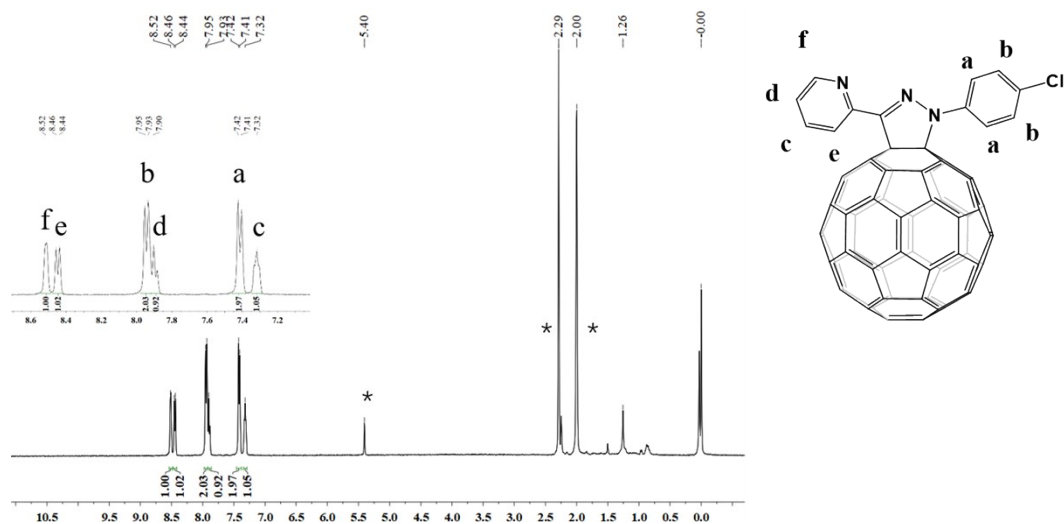


Figure S1. ^1H NMR spectrum of C_{60} -PyP in CS_2/d -acetone solution.

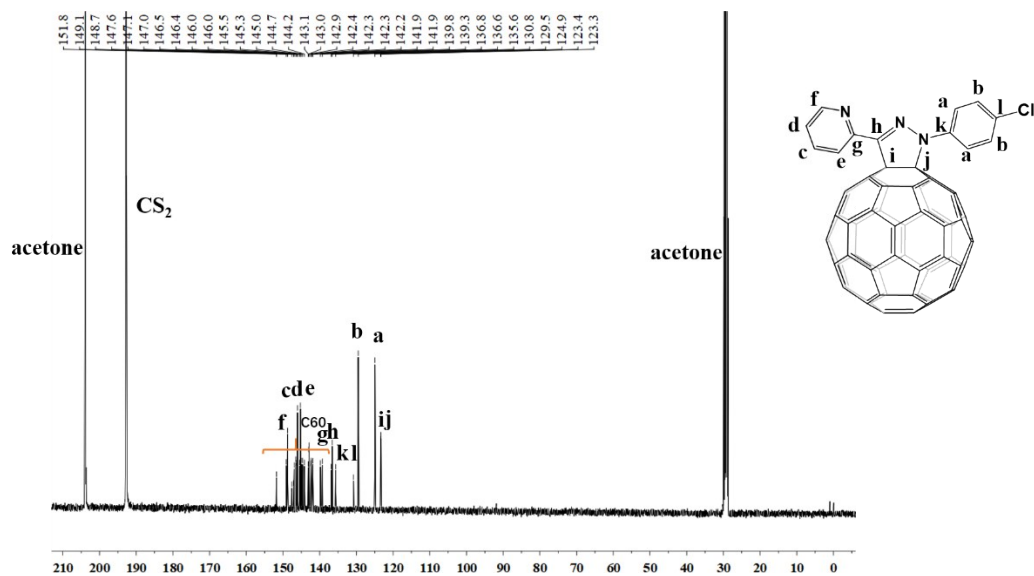


Figure S2. ^{13}C NMR spectrum of C_{60} -PyP in CS_2/d -acetone solution.

S2. Mass spectrum of C₆₀-PyP.

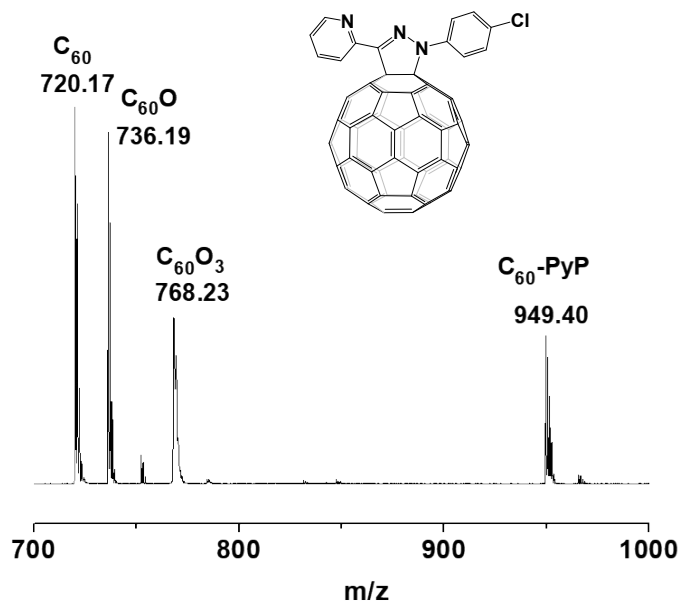


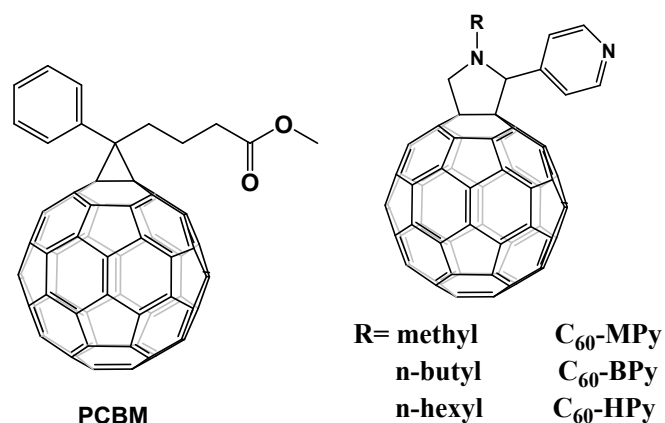
Figure S3. MALDI-TOF Mass spectra of C₆₀-PyP.

S3. Estimation of the energy levels of C₆₀-PyP.

Table S1. Electrochemical data of C₆₀-PyP and PCBM.

	$\lambda_{\text{onset}}^{\text{a}}$ (nm)	$E_{\text{g,opt}}^{\text{b}}$ (eV)	$E_{\text{red,onset}}^{\text{c}}$ (eV)	$E_{\text{LUMO}}^{\text{d}}$ (eV)	$E_{\text{HOMO}}^{\text{e}}$ (eV)
C ₆₀ -PyP	723	1.72	-0.94	-3.89	-5.61
C ₆₀ -MPy	724	1.71	-1.00	-3.80	-5.51
C ₆₀ -Bpy	724	1.71	-0.99	-3.81	-5.52
C ₆₀ -HPy	724	1.71	-0.97	-3.83	-5.54
PCBM	725	1.71	-0.98	-3.82	-5.53

^a Attained from UV-vis spectrum; ^b $E_{\text{g,opt}}=1240/\lambda_{\text{onset}}$; ^c Referred to the half wave potential of ferrocene; ^d $E_{\text{LUMO}}=-e(E_{\text{red,onset}}+4.8\text{ V})$; ^e $E_{\text{HOMO}}=E_{\text{LUMO}}-E_{\text{g,opt}}$



The structure of PCBM and C₆₀-Py.

The energy levels of the lowest unoccupied molecular orbital (LUMO) and highest occupied molecular orbital (HOMO) of the fullerene derivatives were estimated by a cyclic voltammetry study in combination with UV-Vis absorption spectroscopy. Cyclic voltammetry study was performed in *o*-dichlorobenzene with a CHI 630D potentiostat (CHI Instrument, U.S.A.) at room temperature. The supporting electrolyte was tetrabutylammonium perchlorate (TBPA, electrochemical grade, Fluka). A standard three-electrode arrangement of a platinum (Pt) wire as counter electrode, a platinum coil as working electrode, and a saturated calomel electrode as a pseudo-reference electrode was used. In a comparison experiment, ferrocene (Fc) was added as the internal standard and all potentials are referred to the Fc⁺/Fc couple.

The onset reduction potentials ($E_{\text{red, onset}}$) of C₆₀-PyP, C₆₀-BPy was estimated to be -0.94 V vs Fc⁺/Fc. Thus, the LUMO energy levels of C₆₀-PyP was calculated by $E_{\text{LUMO}} = -e(E_{\text{red, onset}} + 4.8)$. The HOMO energy level of C₆₀-PyP was calculated by $E_{\text{HOMO}} = E_{\text{g, opt}} - E_{\text{LUMO}}$,¹ where $E_{\text{g, opt}}$ is the optical bandgap. Based on the onset (λ_{onset}) of UV-vis absorption spectrum of C₆₀-PyP (~723 nm, see Fig. 2b), $E_{\text{g, opt}}$ is estimated to be ~ 1.72 eV, according to the equation: $E_{\text{g, opt}} = 1240/\lambda_{\text{onset}}$.² Therefore, the HOMO energy levels of C₆₀-PyP was estimated to be -5.61 eV. The data of PCBM and C₆₀-Py are quoted from Ref. S2.

S4. TGA analysis of C₆₀-PyP.

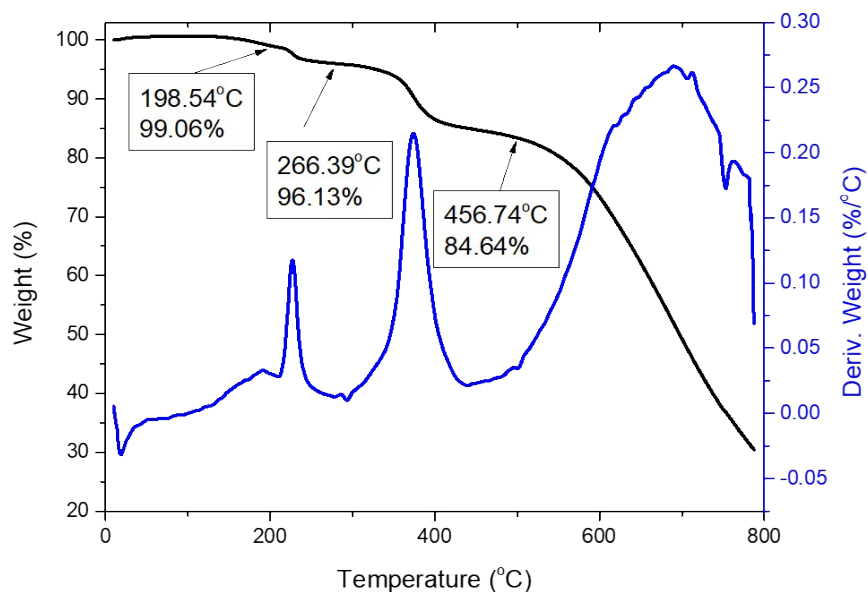


Figure S4. TGA curve (solid line) and differential thermo-gravimetric (DTG) curve (dashed line) of C₆₀-PyP.

S5. UV-vis spectra of the MAPbI₃ perovskite with varying C₆₀-PyP concentration.

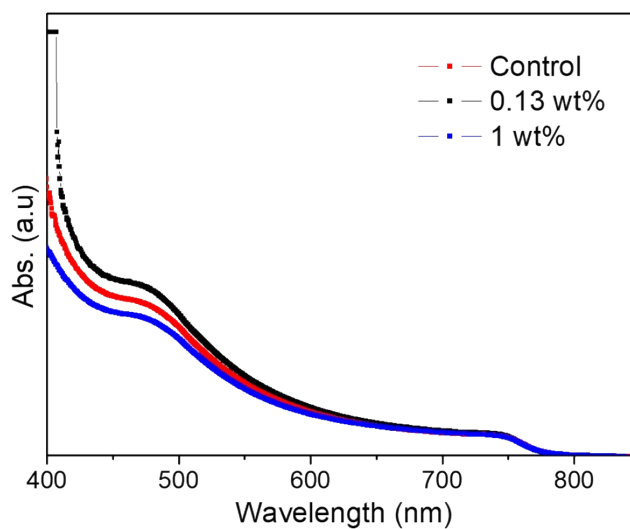


Figure S5. UV-vis spectra of the MAPbI₃ perovskite with varying C₆₀-PyP concentration.

S6. PCE histograms of the control and 0.13 wt% devices.

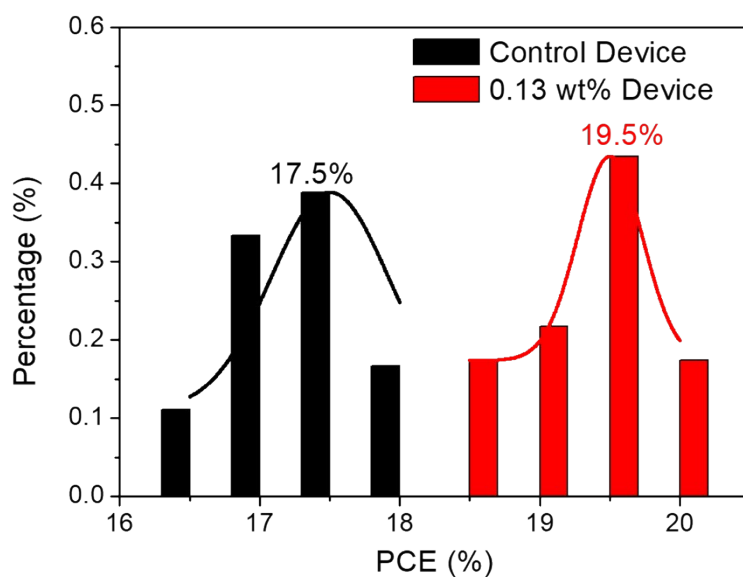


Figure S6. PCE histograms of the control and 0.13 wt% devices.

S7. Photovoltaic parameters box plots of devices with varying C₆₀-PyP concentration.

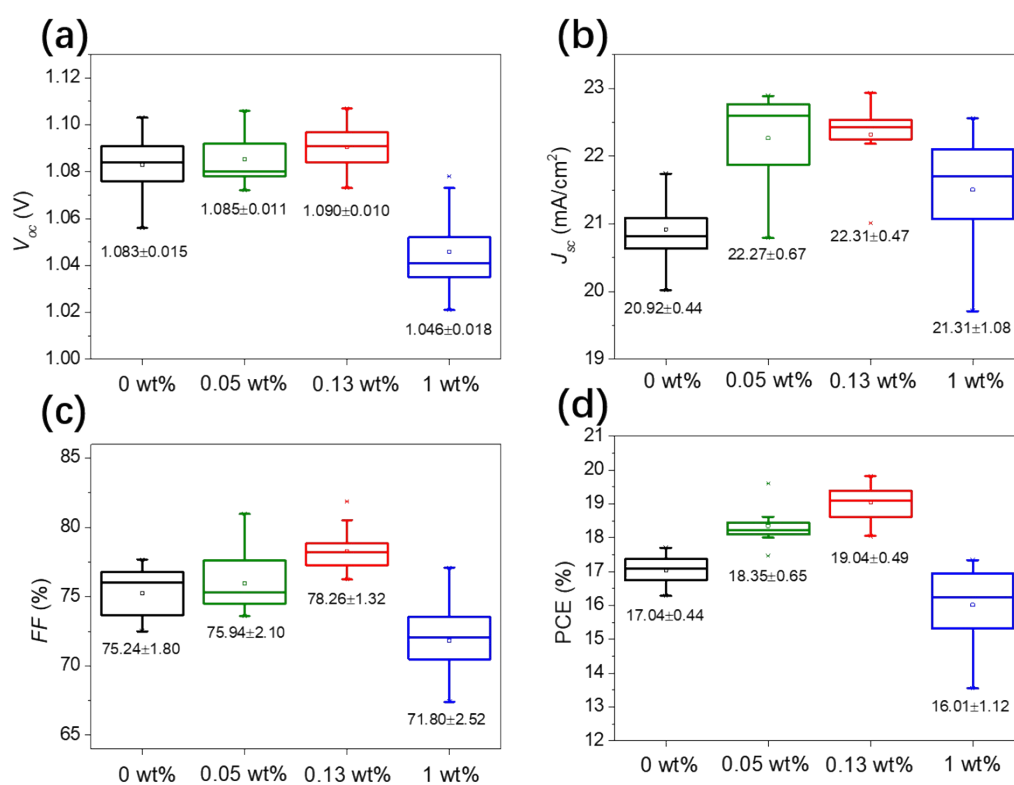


Figure S7. Box plots of V_{oc} (a), J_{sc} (b), FF (c) and PCE (d) for PSC devices with varying C₆₀-PyP concentration.

S8. Hysteresis characterization of devices with and without 0.13 wt% C₆₀-PyP.

Table S2. Photovoltaic parameters of the devices in different scan directions with 0.1 V/s scan rate.

Device	Scan direction	V_{oc} (V)	J_{sc} (mA/cm ²)	FF (%)	PCE (%)	Hysteresis Factor ^a (%)
0%	reverse	1.082	21.01	73.65	16.74	20.3%
	forward	1.038	19.87	64.67	13.35	
0.13 wt%	reverse	1.092	22.25	77.26	18.77	0.53%
	forward	1.088	22.46	76.44	18.67	

^a Hysteresis Factor = [PCE (reverse) – PCE (forward)]/PCE (reverse)

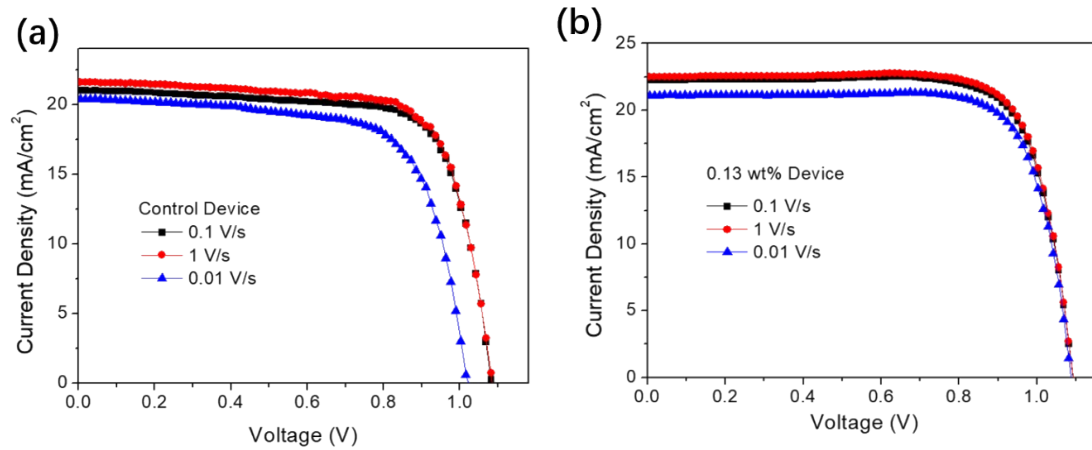


Figure S8. J-V curves of the control (a) and 0.13 wt% (b) devices with different scan rates. The measurements were carried out under illumination of an AM 1.5 solar simulator (100 mW•cm⁻²) in air.

Table S3. Photovoltaic parameters of the control and 0.13 wt% PSC devices with different scan rates.

Device	Scan Rate	V_{oc} (V)	J_{sc} (mA/cm ²)	FF (%)	PCE (%)	R_s (Ω •cm ²)	R_{sh} (Ω •cm ²)
Control	0.01V/s	1.031	20.40	70.20	14.77	13.43	1556.63
	0.1V/s	1.082	21.01	73.65	16.74	5.06	1170.35
	1V/s	1.084	21.60	72.50	16.98	5.43	1208.30
0.13 wt%	0.01V/s	1.087	21.10	77.65	17.81	4.68	7201.70
	0.1V/s	1.092	22.25	77.26	18.77	4.41	3584.64
	1V/s	1.093	22.50	77.50	19.05	4.46	3991.21

S9. Histograms of grain size distributions of the MAPbI₃ perovskite film with varying C₆₀-PyP concentration.

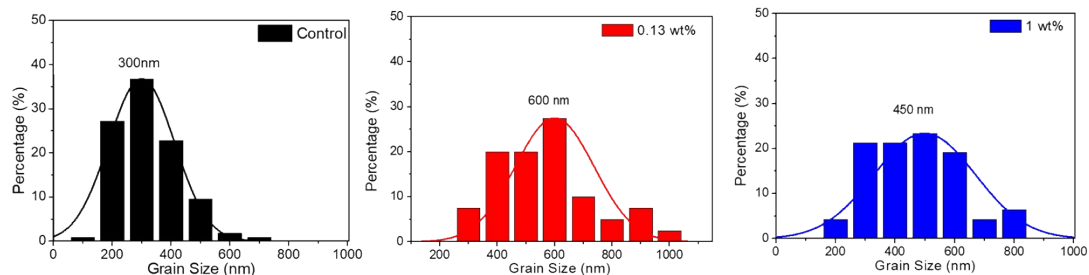


Figure S9. Histograms of grain size distributions of the MAPbI₃ perovskite film with varying C₆₀-PyP concentration.

S10. XPS profile of I 3d of the CH₃NH₃PbI₃ perovskite films without and with 1.0 wt% C₆₀-PyP doping.

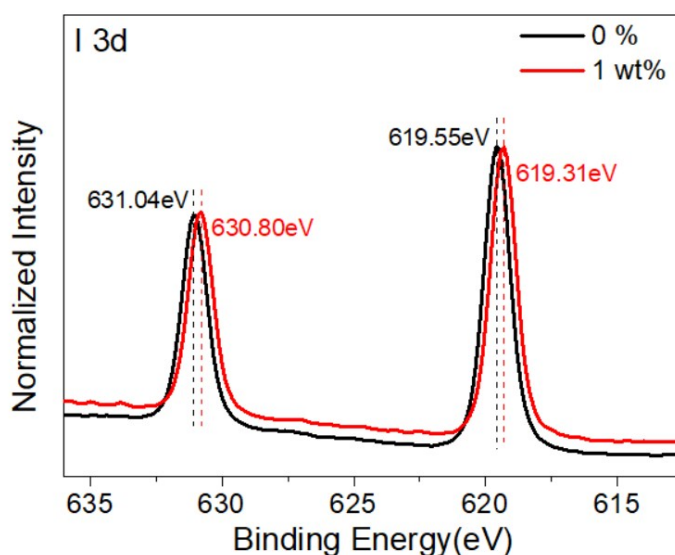


Figure S10. I 3d XPS spectra of the CH₃NH₃PbI₃ perovskite films without and with 1.0 wt% C₆₀-PyP doping.

S11. Analysis of time-resolved photoluminescence (TRPL) spectra of the perovskite films with or without C₆₀-PyP.

The excitation source was a 543 nm picosecond laser pulse which was filtered from a super continuum generation. The TRPL spectrum can be fitted by a single-exponential decay function as shown in equation (S1):^[3-5]

$$f(t) = A \cdot \exp\left(\frac{-t}{\tau}\right) + B \quad (\text{S1})$$

Where A, τ and B are the decay amplitude, the decay lifetime, and a constant for the baseline offset, respectively. The pristine MAPbI₃ perovskite film shows a lifetime of

$\tau = 39.41$ ns, which is similar to those reported values for perovskite film fabricated under similar conditions. After the addition of C₆₀-PyP, the τ value dramatically increases to 8.82.

S12. Fitted EIS data for Control and 0.13 wt% devices.

From the Nyquist plot (Figure 5f), the impedance spectra were fitted with one R-CPE arcs, which a resistor R_s (series resistance) and parallel with an R-CPE elements. R_s is determined by the starting point at the real part of the Nyquist plot. The R_{ct} (charge transfer resistance) is related to the charge transfer dynamics of devices, CPE is the non-ideal chemical capacitances.

Table S4. Fitted EIS data for Control and 0.13 wt% devices.

Device	R_s ($\Omega \cdot \text{cm}^2$)	R_{ct} ($\Omega \cdot \text{cm}^2$)	CPE-T (F/cm ²)	CPE-P
Control	2.802	32.45	3.12E-07	0.993
0.13wt%	1.385	23.71	3.24E-07	0.989

S13. J-V curves and the stabilized photocurrent densities and power outputs measured at the maximum power.

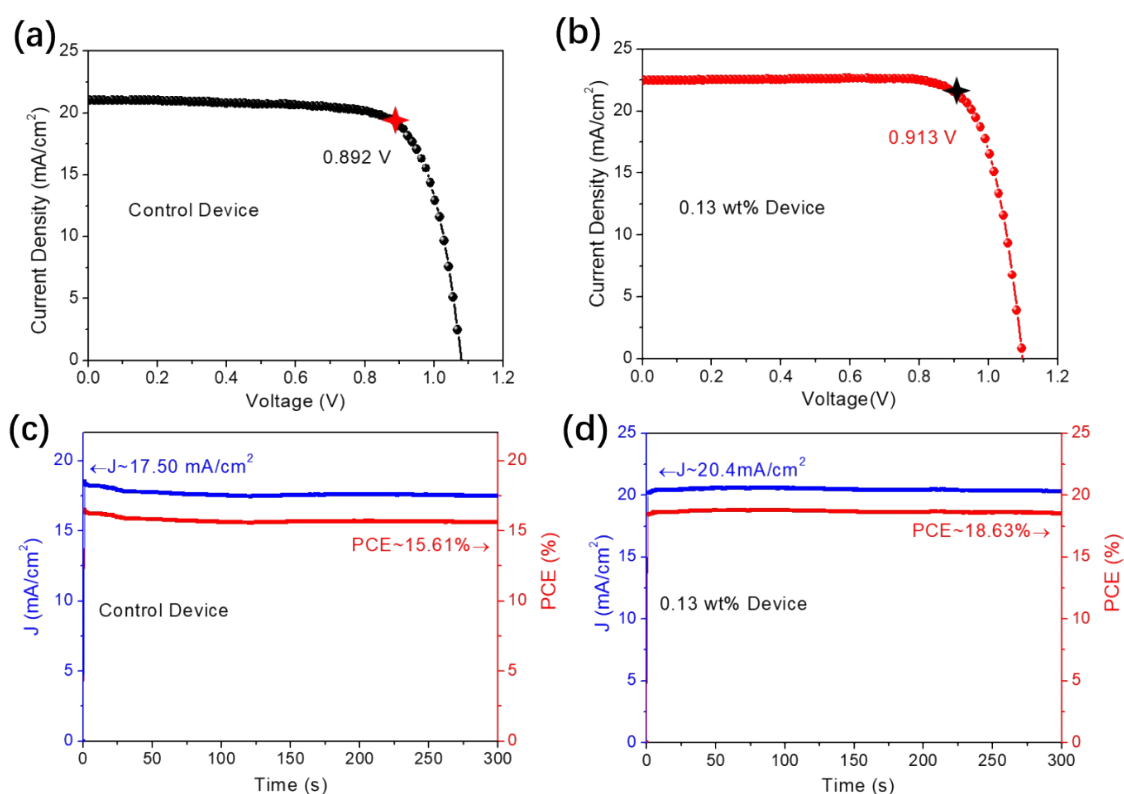


Figure S11. J-V curves (a-b) and the stabilized photocurrent densities and power outputs (c-d) measured at the maximum power points (labelled in curves a-b) of the control and 0.13 wt% devices. For J-V curve measurements, the scanning direction is from open-circuit voltage to short circuit (reverse) and the measurements were carried out with 0.1 V/s scan rate.

Table S5. Photovoltaic parameters of the Control and 0.13 wt% devices

Device	V_{oc} (V)	J_{sc} (mA/cm ²)	FF (%)	PCE (%)	Maximum power point (V)	Stabilized J (mA/cm ²)	Stabilized PCE (%)
Control	1.079	21.03	75.14	17.05	0.892	17.50	15.61
0.13 wt%	1.098	22.47	78.84	19.45	0.913	20.40	18.63

S14. Ambient stabilities of the control and C₆₀-PyP doped perovskite films.

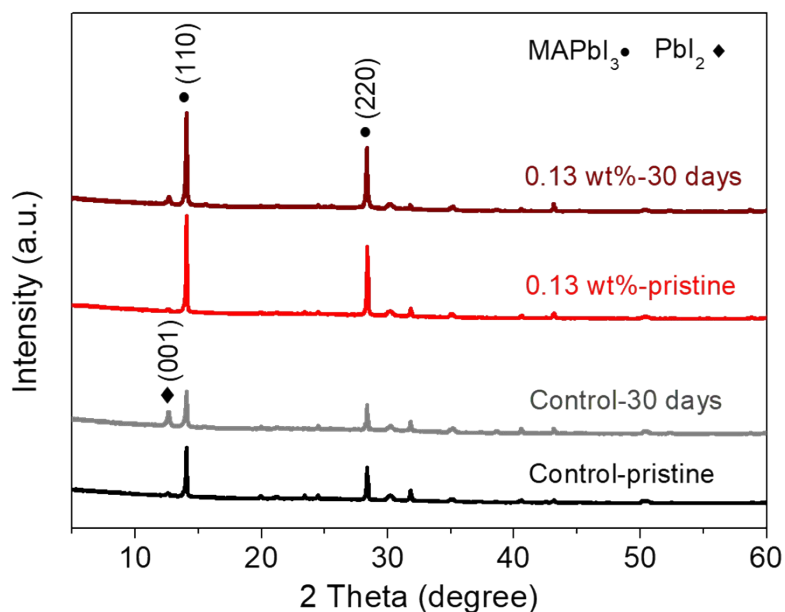


Figure S12. XRD patterns of the control and 0.13 wt% perovskite films before and after ambient storage for 30 days.

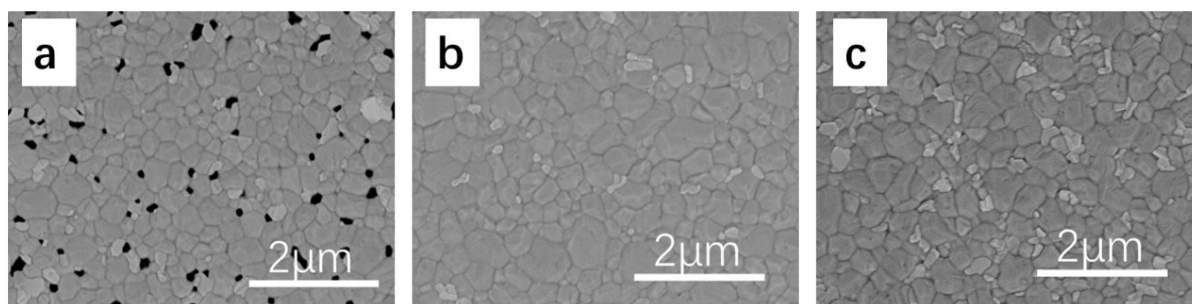


Figure S13. Surface topographic SEM of the MAPbI₃ perovskite film with varying C₆₀-Pyridine concentration after storage for 24h at 80% humidity. (a) Pristine film without C₆₀-PyP, (b) with 0.13 wt% C₆₀-PyP, and (c) with 1 wt% C₆₀-PyP.

Reference:

- (1) H. Wang, W. Zhang, C. Xu, X. Bi, B. Chen and S. Yang, *ACS Appl. Mater. Inter.*, 2013, **5**, 26-34.
- (2) B. Li, J. Zhen, Y. Wan, X. Lei, Q. Liu, Y. Liu, L. Jia, X. Wu, H. Zeng, W. Zhang, G. W. Wang, M. Chen and S. Yang, *ACS Appl. Mater Interfaces*, 2018, **10**, 32471-32482.
- (3) Y. Lin, L. Shen, J. Dai, Y. Deng, Y. Wu, Y. Bai, X. Zheng, J. Wang, Y. Fang, H. Wei, W. Ma, X. C. Zeng, X. Zhan and J. Huang, *Adv. Mater.*, 2017, **29**, 1604545.

- (4) J. W. Jung, C.-C. Chueh and A. K.-Y. Jen, *Adv. Energy Mater.*, 2015, **5**, 1500486.
- (5) P.-W. Liang, C.-Y. Liao, C.-C. Chueh, F. Zuo, S. T. Williams, X.-K. Xin, J. Lin and A. K.-Y. Jen, *Adv. Mater.*, 2014, **26**, 3748-3754.